

Geomagnetic Effects on Atmospheric Neutrinos

Paolo Lipari², Todor Stanev¹ & T.K. Gaisser¹

¹Bartol Research Institute

University of Delaware, Newark, DE 19716

² Dipt. di Fisica and INFN

Università di Roma I, Piazzale A. Moro 2

00185 Roma, Italy

Abstract

Geomagnetic effects distort the zenith angle distribution of sub-GeV and few-GeV atmospheric neutrinos, breaking the up-down symmetry that would be present in the absence of neutrino oscillations and without a geomagnetic field. The geomagnetic effects also produce a characteristic azimuthal dependence of the ν -fluxes, related to the well known east-west effect, that should be detectable in neutrino experiments of sufficiently large mass. We discuss these effects quantitatively. Because the azimuthal dependence is in first order independent of any oscillation effect, it is a useful diagnostic tool for studying possible systematic effects in the search for neutrino oscillations.

I. INTRODUCTION

The flux of atmospheric neutrinos at a fixed value of the energy E_ν depends both on the zenith and azimuth angles (θ_z and φ). The angular dependence originates from two, or possibly three sources:

1. The development of cosmic ray showers in the atmosphere.
2. Geomagnetic effects on the primary cosmic ray flux.
3. Neutrino oscillations.

The development of an hadronic shower induced by a primary particle of given energy and mass depends only on the zenith angle. Cascades at large zenith angle develop in a relatively less dense part of the atmosphere, so that decay to neutrinos is enhanced at large angle. In fact, the calculation of the secondary beam depends only on $|\cos \theta_z|$ because a line of sight entering the detector from below the horizon with zenith angle $\theta_z^{out} > \pi/2$, corresponds to a trajectory entering the atmosphere with $\theta_z^{in} = \pi - \theta_z^{out}$. Apart from small effects due to the different average temperature profiles of the atmosphere at different geographical locations, the development of a shower does not depend on the position of its impact point on the earth's surface. Thus, production of secondary particles in the atmosphere is symmetric under the reflection $\cos \theta_z \leftrightarrow -\cos \theta_z$.

For a given energy spectrum, neutrino oscillations also depend only on zenith angle; however, the dependence is strongly asymmetric because the pathlengths corresponding to the directions $\pm \cos \theta_z$ are very different. For down-going particles, the neutrino pathlengths are in the range from ~ 10 to ~ 500 km [1], whereas up-going neutrinos have $L \sim 10^4$ km.

Geomagnetic effects modify the spectrum of primary cosmic rays up to tens of GeV in a way that depends on azimuth as well as zenith. Since the neutrino flux is a convolution of the primary spectrum with the yield of neutrinos per primary particle, neutrinos with energies below a few GeV carry the imprint of these geomagnetic effects. The geomagnetic field prevents primary cosmic rays of low rigidity from reaching the atmosphere. This suppression

depends on both the detector location, being lowest (highest) at the magnetic poles (equator), and on the line of sight considered. For directions from below the horizon the effect must obviously be calculated for the geomagnetic field at the position where the cosmic-ray trajectories enter the volume of the atmosphere. The nuclear component of cosmic rays is positively charged, and this introduces a dependence on the azimuth angle, the celebrated east–west effect. The neutrino flux is highest (lowest) for directions coming from the west (east).

For most interactions of atmospheric neutrinos in present detectors the direction of the neutrino is not fully reconstructed. Typically, the direction of the charged lepton will be used to indicate the direction of the event. For detected leptons with momenta in the interval $0.2 \leq E_{\mu,e} \leq 1$ GeV the east–west asymmetry is of order 30%, after taking into account the dilution of the effect due to the broad distribution of angles between the charged lepton and the neutrino. An effect of this size should be readily measurable by high statistics experiments. For events in the multi–GeV range, when the initial neutrino energy is of order of several GeV the east-west effect is reduced to $\sim 10\%$. For a detailed study it is necessary to consider the exact geographical location of the detector, and the interval of neutrino energy that is detected.

In the presence of neutrino oscillations the zenith angle distribution of the detected events can be significantly deformed; however, the asymmetry in azimuth remains unchanged to first order because the neutrino pathlength does not depend on φ . Only to second order would the deformation of the neutrino energy spectrum by oscillations lead to a slight modification of the distribution in azimuth. The azimuthal distribution depends only on the filtering of the primary cosmic rays through the geomagnetic field as viewed from each detector. Study of the azimuthal dependence of neutrino interactions can therefore be a valuable diagnostic tool, both to validate calculations of the neutrino flux and to check the quality of detector performance, for example, to demonstrate that the determination of the lepton directions has the expected resolution. Moreover, since the geomagnetic effects are the only known mechanism (besides ν –oscillations) that can produce an up–down asymmetry

for the neutrino fluxes, a measurement of the east–west effect for neutrinos would establish the size of the geomagnetic effects, and greatly help in limiting the possible importance of geomagnetic effects on the zenith angle distributions. The existence of distortions of the zenith angle distributions due to neutrino oscillations could then be more clearly identified.

This discussion can be summarized in the following equation:

$$\phi_{\nu_\alpha}(E_\nu, \Omega_\nu, \vec{x}_d) = \sum_A \phi_A(E_0) F_M[p_0/Z, \Omega_0, \vec{x}(\Omega_0)] \times \sum_\beta \frac{dn_{\nu_\beta}}{dE_\nu}(E_\nu, A, E_0, |\cos \theta_z|) \langle P_{\nu_\beta \rightarrow \nu_\alpha}(E_\nu, \cos \theta_z, \{m_j^2, U_{\alpha j}\}) \rangle \quad (1)$$

where $\phi_{\nu_\alpha}(E_\nu, \Omega_\nu, \vec{x}_d)$ is the flux of neutrinos of flavor α with energy E_ν and direction Ω_ν observable in a detector located at a position \vec{x}_d . $\phi_A(E_0)$ is the flux of primary cosmic rays of energy E_0 in the vicinity of the earth, but at a distance r sufficiently large so that the effects of the geomagnetic field are negligible ($r \gtrsim 10 r_\oplus$, where r_\oplus is the radius of the earth). This flux is isotropic to a very good approximation. The cutoff factor F_M takes into account the effects of the geomagnetic field. It depends on the rigidity $R = p_0/Z$ and direction Ω_0 of the primary particle and on the position \vec{x}_{in} where its trajectory first intersects the atmosphere. dn_{ν_β}/dE_ν is the average number of neutrinos of flavor β produced by a primary particle of mass A and energy E_0 . It depends on the mass, energy and zenith angle of the primary particle. Finally, $\langle P_{\nu_\beta \rightarrow \nu_\alpha} \rangle$ is the oscillation probability for the transition $\nu_\beta \rightarrow \nu_\alpha$ averaged over the position of creation of the neutrinos. It depends on the energy and trajectory of the neutrino and on the oscillation parameters; that is, the mass eigenvalues m_j and the mixing matrix $U_{\alpha j}$ that relates mass and flavor eigenstates.

We first discuss the calculation of the probability of penetration through the geomagnetic field. Then in §3 we describe the Monte Carlo convolution expressed in Eq. 1. Results and discussion follow.

II. GEOMAGNETIC EFFECTS

To a first approximation the effects of the field can be described simply by a cutoff rigidity $R_c(\vec{x}_d, \Omega)$, which is a function of the detector position \vec{x} and the direction Ω , such that all rigidities smaller (larger) than R_c are forbidden (allowed); that is:

$$F_M(R, \Omega, \vec{x}_d) = \Theta[R - R_c(\theta_z, \varphi, \vec{x}_d)], \quad (2)$$

where $\Theta(x)$ is the Heavyside function ($\Theta(x) = 0$ for $x < 1$, $\Theta(x) = 1$ for $x \geq 1$).

In the case of a dipolar magnetic field that fills the entire space, it is possible to compute the cutoff rigidity exactly:

$$R_c = R_S(r, \lambda_M, \theta_z, \varphi) = \left(\frac{M}{2r^2} \right) \left\{ \frac{\cos^4 \lambda_M}{[1 + (1 + \cos^3 \lambda_M \sin \theta_z \sin \varphi)^{1/2}]^2} \right\}, \quad (3)$$

where M is the magnetic dipole moment, r (the distance from the dipole center) and λ_M (the magnetic latitude) describe the detector position, θ_z is the zenith angle and φ is an azimuthal angle, with $\varphi = 0$ ($\frac{\pi}{2}$) indicating the north (west) direction. For the earth $M \simeq 8.1 \times 10^{25}$ Gauss cm³, which corresponds to a polar magnetic field of 0.62 Gauss. The quantity $M/(2r_\oplus^2) \simeq 59.4$ GV corresponds to the rigidity of a particle in a circular orbit of radius r_\oplus in the earth's magnetic equatorial plane.

Stormer's formula (Eq. 3) gives a good idea of the magnitude of the geomagnetic cutoffs, but it has limited accuracy because the geomagnetic field is only approximately an offset dipole. The formula also generally underestimates the cutoffs because it neglects the shadow of the Earth, i.e. allows the penetration of charged particles with trajectories that would have intersected the surface of the Earth. More exact calculations can be done using the backtracking technique [2] and more realistic models of the geomagnetic field [3].

In the backtracking technique, to establish if a particle with charge Z and momentum p traveling from interplanetary space can reach a final point \vec{x} close to the surface of the earth arriving from the direction Ω , one integrates the equation of motion for a particle with opposite charge and reflected momentum starting from this final position. If the backtracked

anti-particle reaches infinity, we can assume that the trajectory is allowed ($F_M = 1$), if the backtracked particle is trapped in the geomagnetic field or if its trajectory intersects the surface ($r = r_{\oplus}$) the trajectory is considered forbidden ($F_M = 0$). Such a calculation was performed in Ref. [4], considering as ‘trapped’ those trajectories that remained confined within $r \leq 30 r_{\oplus}$ for a pathlength longer $l \geq 500 r_{\oplus}$. Instead of the sharp rigidity cutoff predicted by equation 3, above which all particles from a particular direction reach the atmosphere, one encounters a quite different situation: in the vicinity of R_S particle trajectories change rapidly with the rigidity, and the sharp cutoff is replaced with a series of allowed ($F_M = 1$) and disallowed ($F_M = 0$) rigidities – the penumbra region.

The function F_M used in this paper is calculated by backtracking particles for a set of rigidities at $\Delta \cos \theta_z$ of 0.02 and $\Delta \phi$ of 5° . The results are then averaged for angular bins of $\Delta \cos \theta_z = 0.1$ and $\Delta \phi$ of 30° , i.e. using the cutoffs for 36 directions for every rigidity value. The cutoffs are thus replaced with the probability per angular bin for a cosmic ray of given rigidity to reach vertical altitude of 20 km and interact in the atmosphere.

III. MONTECARLO CALCULATION

The calculation of the neutrino flux that we use here is described in Refs. [5,6]. Yields of neutrinos are calculated separately for a grid of energies for primary protons and neutrons. In the energy range of interest here, approximately 80% of the incident nucleons are free protons. Most of the rest are neutrons and protons in primary alpha particles. For each direction (20 bins of $\cos \theta_z$ and 12 bins of ϕ) the yields are folded with the primary spectrum to obtain the neutrino flux. The primary spectrum is weighted with the cutoffs averaged over the $\cos \theta_z$ – ϕ bin.

We assume that the neutrinos are collinear with the primary cosmic ray particles that produce them. The angle $\theta_{0\nu}$ of the neutrino with respect to the shower axis, for approximately half of the muon neutrinos, can be schematically written as: $\theta_{0\nu} = \theta_{\pi} \oplus \theta_{\pi\nu}$, where θ_{π} is the angle between the parent meson (most of the time a charged pion) and the primary

particle, and $\theta_{\pi\nu}$ the angle between the meson and the neutrino; for electron neutrinos and for the other half of the muon neutrinos one has to consider a two-decay chain, and the angle between primary particle and neutrinos is $\theta_{0\nu} = \theta_\pi \oplus \theta_{\pi\mu} \oplus \theta_{\mu\nu}$. Since the maximum p_\perp kinematically allowed in a π^\pm (μ^\pm) decay is 30 (50) MeV, the dominant contribution to the neutrino angle comes from the transverse momentum of the parent meson (of order 300 MeV):

$$\langle \theta_{0\nu} \rangle \simeq \langle \theta_\pi \rangle \simeq \frac{\langle p_{\perp,\pi} \rangle}{E_\pi} \simeq \frac{300 \text{ MeV}}{4 E_\nu} \simeq \frac{4.3^\circ}{E_\nu(\text{GeV})} \quad (4)$$

where we have used the fact that on average the neutrino has approximately one-quarter of the parent pion energy. The angle $\theta_{0\nu}$ is smaller than the angle $\theta_{\ell\nu}$ between the detected charged lepton and the neutrino, and its neglect does not introduce significant errors in the predictions of the geomagnetic effects on the angular distribution of the charged leptons.

The next step is to treat the interaction of the neutrinos in the detector and find the direction of the produced leptons. For this purpose we use the quasi-elastic and single pion neutrino cross sections as calculated in Ref. [7] including corrections for nuclear target. For deep inelastic scattering we use the structure functions of Ref. [8]. Neutral current interactions are neglected. The direction of each neutrino is chosen randomly within the bin and the direction of the outgoing electron or muon is then chosen randomly using the appropriate differential cross section.

To provide realistic and relevant examples of the angular dependence, we consider two classes of events, applying cuts similar to those of Super-Kamiokande (SK) [9]. As a low-energy sample, we use quasi-elastic simulated events in which electrons (muons) have momenta in the interval $0.1 < p_e < 1.33 \text{ GeV}/c$ ($0.2 < p_\mu < 1.33 \text{ GeV}/c$). We compare this low energy sample to the ‘single-ring’ subset of the sub-GeV data of SK. As a high-energy sample, we compare all events with lepton momenta in the interval $1.33 < p_\ell < 10 \text{ GeV}$ with the multi-GeV data of SK. Our definitions are of course not precisely equivalent to the experimental classifications. For example, the single-ring events in the data include some multi-particle events in which only one is visible. Conversely, some quasi-elastic events

would be excluded from the single-ring sample because of an energetic recoil proton. We did check that both these contributions are small and that they do not significantly alter the angular distributions of leptons. Thus we believe that the simplified cuts we make on the Monte Carlo are adequate for our purposes to illustrate the expected angular dependence of the two categories of leptons. As a confirmation, we can compare the number of events in our cuts with the corresponding cuts in the SK data. We find 689 sub-GeV electrons and 1050 sub-GeV muons (single ring only) as compared to 789 and 1185 in 25.5 kT-years that the Super-Kamiokande Collaboration report [9] from their simulation using the same neutrino flux. For the same exposure, we find a total of 1034 multi-GeV leptons as compared to 1176 in the SK simulation.

We show in Fig. 1a the distributions of neutrino energies that give rise to the two classes of events. The average neutrino energy for our sub-GeV muon sample is 0.8 GeV as compared to 5.7 GeV for the higher energy class. The order-of-magnitude difference in energy corresponds to a similar difference in L/E and makes the atmospheric neutrino beam a powerful probe of oscillations in an interval of parameter space with large mixing and $10^{-3} \leq \Delta m^2 \leq 10^{-2}$ eV 2 . This follows from the well-known expression for survival of a neutrino flavor in vacuum, which in a two-neutrino example is

$$P_{\nu_\beta \rightarrow \nu_\alpha} = 1 - \sin^2 2\theta \sin^2 \left[1.27 \frac{\Delta m^2 (eV^2) L_{km}}{E_{GeV}} \right], \quad (5)$$

together with the large differences in pathlength between up-going and down-going neutrinos.

In Fig. 1b we show the distribution of the angle between the detected muon and the parent neutrino. The average values of $\cos \theta$ for the sub- and multi-GeV samples are 0.53 and 0.97 respectively. Normally only the charged lepton is detected, and because of the angle $\theta_{\ell\nu}$ with respect to the parent neutrino direction there is a smearing of the angular distribution of the neutrinos which is significant for the sub-GeV sample. Only detectors with high granularity can measure the recoiling nucleons (or more complicated hadronic final states) and reconstruct the neutrino energy and direction. Such a measurement is

potentially highly valuable in the search for neutrino oscillations.

We illustrate the effect of the angular smearing in Fig. 2 by showing the azimuthal and zenith angle distributions for sub-GeV muons (solid lines) as compared to the same distributions for their parent neutrinos (dotted lines) at the location of SK. The azimuth is defined so that 0° corresponds to events from the north. Azimuthal angle increases counter-clockwise. The most prominent feature is the excess of events from the west. The $\cos \theta_z$ dependence for sub-GeV events at Kamioka is dominated by the high local geomagnetic cutoffs. We understand the slight excess of events from below ($\cos \theta_z < 0$) as arising from the fact that the local geomagnetic cutoffs, which affect the down-going events, are generally higher than the cutoffs averaged over the opposite hemisphere of the earth that regulate the up-going events. We note that both geomagnetic poles are below the horizon at Kamioka and therefore contribute to the relative excess of events for negative $\cos \theta_z$. The depression of the neutrino flux near the horizon indicates that, for the sub-GeV events, the geomagnetic suppression more than compensates for the enhanced production of neutrinos from muon decay in this same angular region.

In Fig. 3 we compare the azimuthal dependence for sub-GeV and multi-GeV events for four intervals of $\cos \theta_z$ of equal solid angle. The multi-GeV sample is sufficiently high in energy that the geomagnetic effects are much reduced.

IV. RESULTS AND DISCUSSION

Geomagnetic location is of great importance for the nature of the fluxes and angular distributions of low-energy events. We illustrate this in Fig. 4 by comparing the angular distributions expected in the absence of oscillations for sub-GeV muons at Kamioka with that expected at Soudan [10] or SNO [11]. The latter two experiments are near the north geomagnetic pole, so the flux of down-going events is significantly higher than at Kamioka. Moreover, the east-west effect is nearly absent for events coming from above. The sky-maps are in local coordinates with the local zenith at the top and the local nadir direction at the

bottom of each map.

The angular-dependence of the neutrino events recently reported from Super-Kamiokande [9] has suggested several interpretations. Among these, the simplest possibilities are $\nu_\mu \leftrightarrow \nu_\tau$ and $\nu_\mu \leftrightarrow \nu_{sterile}$ [12–14]. In Fig. 5 we show the expected zenith angle dependence for sub-GeV and multi-GeV neutrino induced muons at Kamioka (using our definition). The solid line shows the result for no-oscillations. In the multi-GeV sample, the expected enhancement near the horizontal is clearly visible. The three broken lines show the results expected according to Eq. 5 for full mixing assuming $\nu_\mu \leftrightarrow \nu_\tau$ with $\Delta m^2 = 10^{-2}$, $10^{-2.5}$, and 10^{-3} eV². The distortion of the zenith angle distribution produced by neutrino oscillations depends on the oscillation parameters. Vertical up-going muons have the same suppression $\sim 1 - \frac{1}{2} \sin^2 2\theta$ because of the averaging of oscillations on the long pathlength. The shape of the suppression factor as a function of zenith angle depends strongly on Δm^2 and is different in the two samples, reflecting the order of magnitude difference in the typical energy of the neutrinos that give rise to the events. These features are potentially distinguishable with the future high statistics data of Super-Kamiokande.

Whereas the shape of the zenith angle dependence strongly reflects assumptions about oscillations, the azimuthal dependence at fixed zenith is practically the same for all oscillations scenarios. We show this in Fig. 6 for the sub-GeV muons (Kamioka, our definition). The four panels are for regions of equal solid angle of increasing zenith angle from the vertically down-going quadrant to the vertically up-going quadrant. Typical pathlengths in the two down-going quadrants are ~ 30 km and ~ 300 km, with large variations due to neutrino-lepton scattering angle as well as the relatively broad distributions of production height [1]. The up-going quadrants have pathlengths of order 10^4 km, with an admixture of shorter pathlengths near the horizontal direction.

Table 1 gives a quantitative summary of the east–west effect for neutrino induced muons at Kamioka. The west/east ratio is ≈ 1.35 for down-going and ≈ 1.28 for up-going, sub-GeV muons. The ratio is ≈ 1.10 for the multi-GeV muons. These ratios have a negligible dependence on the nature of the assumed oscillation. For this reason, study of the azimuthal

dependence of neutrino interactions should provide an important probe of the systematics of searches for neutrino oscillations with the atmospheric neutrino beam. In addition, study of the azimuthal and zenith angle dependence of electrons should be a sensitive test of whether (as suggested in Refs. [15,14]) oscillations on terrestrial scales also involve electron neutrinos to some extent.

Acknowledgements The authors acknowledge helpful discussions with E. Kearns. PL thanks BRI for its hospitality during the completion of this work. The research of TKG and TS is supported in part by the U.S. Department of Energy under Grant Number DE FG02 01ER 4062.

REFERENCES

- [1] T.K. Gaisser & Todor Stanev, Phys. Rev. D57 (1998) 1977.
- [2] J. W. Bieber, P. Evenson and Z. Lin, *Antarctic J.*, 27, 318 (1992); E.O. Flückiger, E. Kobel, D.F. Smart and M.A. Shea, *Proc. 22nd Int. Cosmic Ray Conf.* (Dublin), 3, 648 (1991); R. Gall *et al.* *Universidad Nacional Autonoma de Mexico*, Mexico City, 1982.
- [3] IGRF, 1991 Revision, EOS, Trans. AGU, 72, 182 (1992).
- [4] Paolo Lipari & Todor Stanev, Proc. 24th Int. Cosmic Ray Conf. (Rome, 1995) Vol. 1, p. 516.
- [5] Vivek Agrawal, T.K. Gaisser, Paolo Lipari & Todor Stanev, Phys. Rev. D53 (1996) 1314.
- [6] T.K. Gaisser & Todor Stanev, Proc. 24th Int. Cosmic Ray Conf. (Rome, 1995) Vol. 1, p. 694.
- [7] P. Lipari, M. Lusignoli, and F. Sartogo, Phys. Rev. Lett. 74, 4384 (1995).
- [8] M. Gluck, E. Reya, and A. Vogt, Z.Phys. C 67, 433 (1995).
- [9] E. Kearns (for the SuperKamiokande Collaboration) (TAUP97 proceedings).
- [10] T. Kafka (for the Soudan Collaboration) hep-ph/9712281 (TAUP97 proceedings).
- [11] The Sudbury Neutrino Observatory, <http://snodaq.phy.queens.ca/SNO/>.
- [12] E. Akhmedov, P. Lipari, and M. Lusignoli, Phys.Lett. B 300, 128 (1993).
- [13] Q.Y. Liu and A.Yu. Smirnov, hep-ph/9712493.
- [14] R. Foot and R.R. Volkas, Phys. Rev. D 52, 6595 (1995); R. Foot, R.R. Volkas and O. Yasuda, hep-ph/9801431.
- [15] P.F. Harrison, D.H. Perkins and W.G. Scott, Phys.Lett. B 396, 186 (1997); Phys.Lett. B 349, 137 (1995).

TABLES

TABLE I. Average muon rates (in units $(\text{Kt yr sr})^{-1}$) in four solid angle quadrants. The rates are calculated in the absence of oscillations and for $\nu_\mu \rightarrow \nu_\tau$ oscillations with maximal mixing and three values of Δm^2 .

Δm^2 (eV 2)	sub-GeV				multi-GeV			
	downgoing		upgoing		downgoing		upgoing	
	west	east	west	east	west	east	west	east
No-osc.	3.56	2.59	3.92	3.06	2.55	2.31	2.55	2.33
10^{-3}	2.98	2.20	2.22	1.70	2.46	2.23	1.38	1.25
$10^{-2.5}$	2.67	2.00	2.08	1.62	2.35	2.15	1.31	1.20
10^{-2}	2.06	1.54	1.94	1.52	2.15	1.98	1.28	1.17

FIGURES

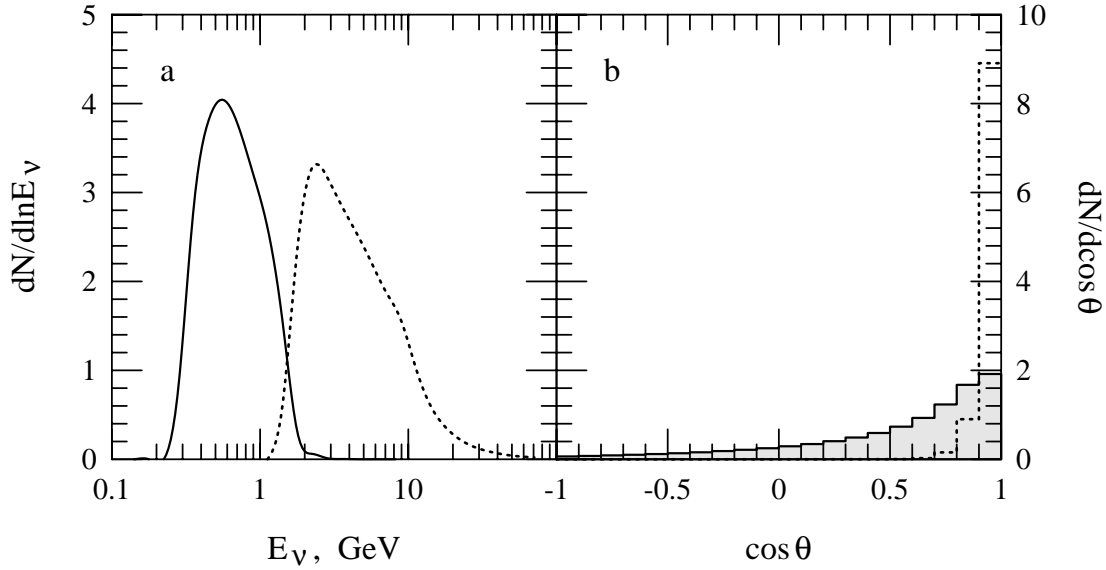


FIG. 1. *a).* Distributions of neutrino energies that give rise to the sub-GeV (solid line) and multi-GeV (dotted line) muon samples at Kamioka – see text for the definitions of the two groups of events in this calculation. *b).* Distribution of $\cos \theta$ (θ is the angle between the neutrino and muon direction) for the same two muon samples, same coding.

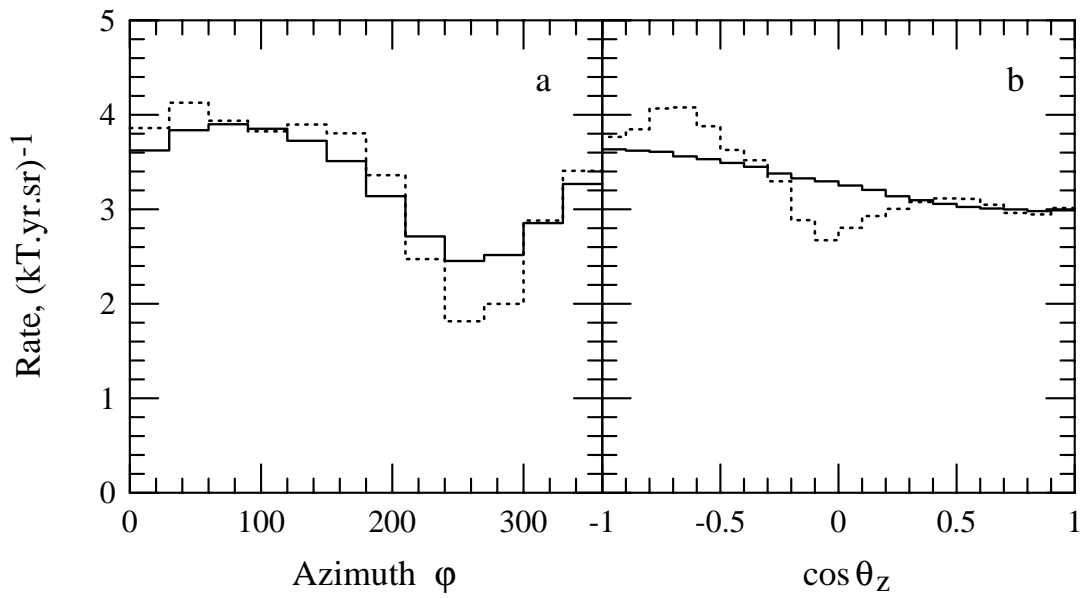


FIG. 2. a) Azimuthal distributions for the sub-GeV muons (see text) at Kamioka (solid line) and for their parent atmospheric neutrinos (dotted line) averaged over the zenith angle θ_z . b) $\cos \theta_z$ distributions (averaged over the azimuth angle φ) for the same muon and neutrino samples.

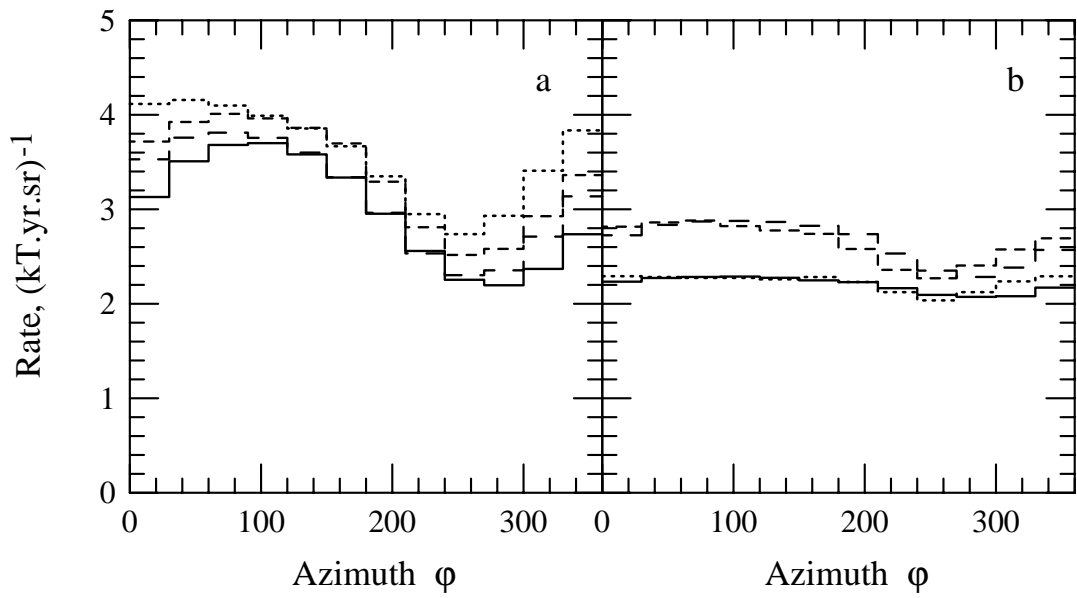


FIG. 3. a) Azimuthal distributions for the sub-GeV muons (see text) at Kamioka for four bins in $\cos \theta_z$: 1 to 0.5 (solid); 0.5 to 0. (dots); 0. to -0.5 (short dash); -0.5 to -1. (long dash). b) Azimuthal distributions for the multi-GeV muons at Kamioka, same coding.

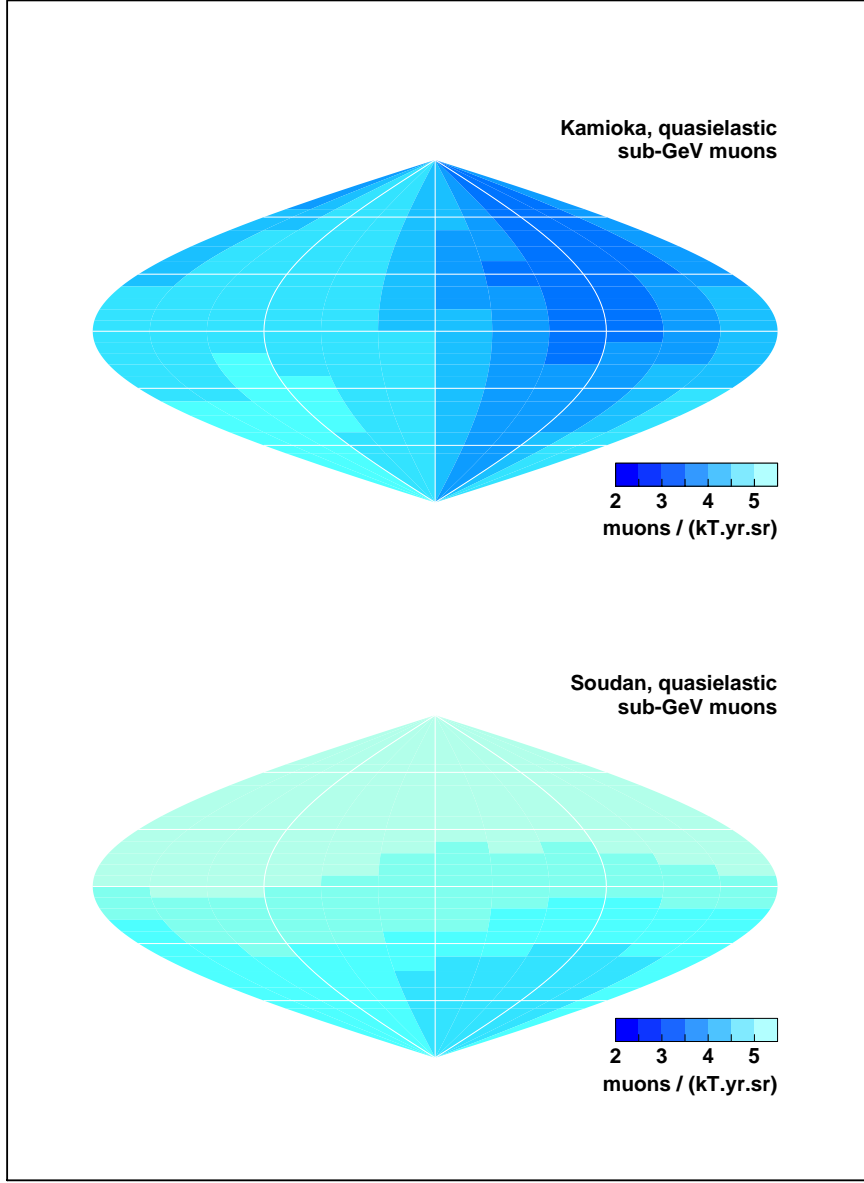


FIG. 4. Two dimensional azimuthal and zenith angle distribution of the sub-GeV muons (see text) at Kamioka (top) and Soudan/SNO (bottom) in units of number of muons per $kT \cdot \text{yr} \cdot \text{sr}$. The top of the maps corresponds to the local zenith and the bottom to the local nadir. The north direction ($\varphi = 0$) corresponds to the edge of the map, south ($\varphi = 180^\circ$) to the vertical line in the middle with west ($\varphi = 90^\circ$) and east ($\varphi = 270^\circ$) to the left and right. Notice the smeared east-west effect in both maps.

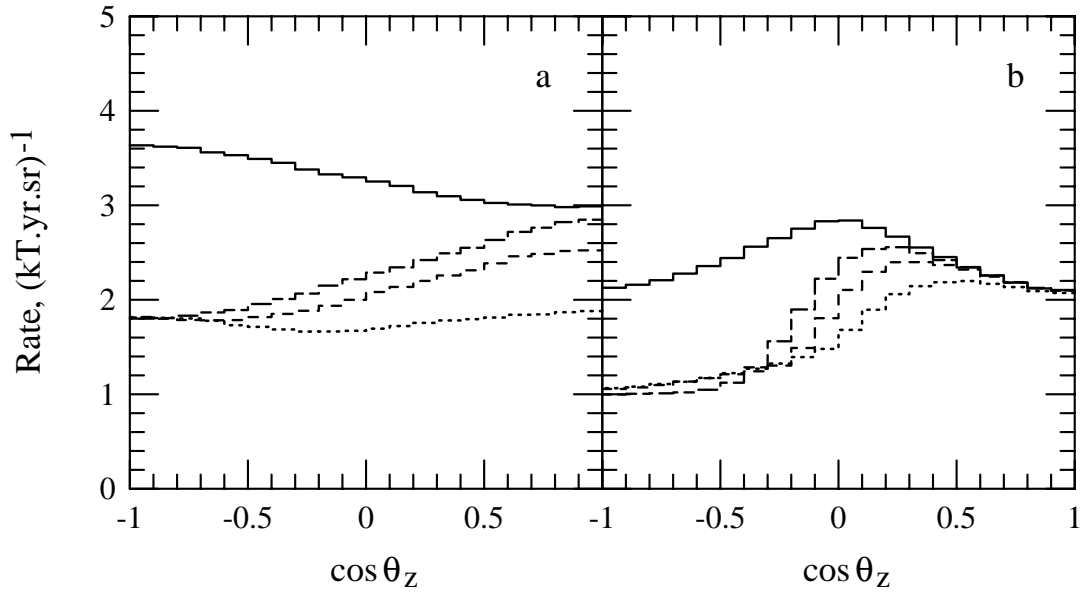


FIG. 5. a) $\cos \theta_z$ distribution for the sub- GeV muons (see text) at Kamioka, averaged over azimuth – solid line. The other histograms are for $\nu_\mu \rightarrow \nu_\tau$ oscillations with maximal mixing and $\Delta m^2 = 10^{-2} \text{ eV}^2$ (dots), $10^{-2.5} \text{ eV}^2$ (dashes) and 10^{-3} eV^2 (dash-dash). b) The same distributions for multi- GeV muons, same coding.

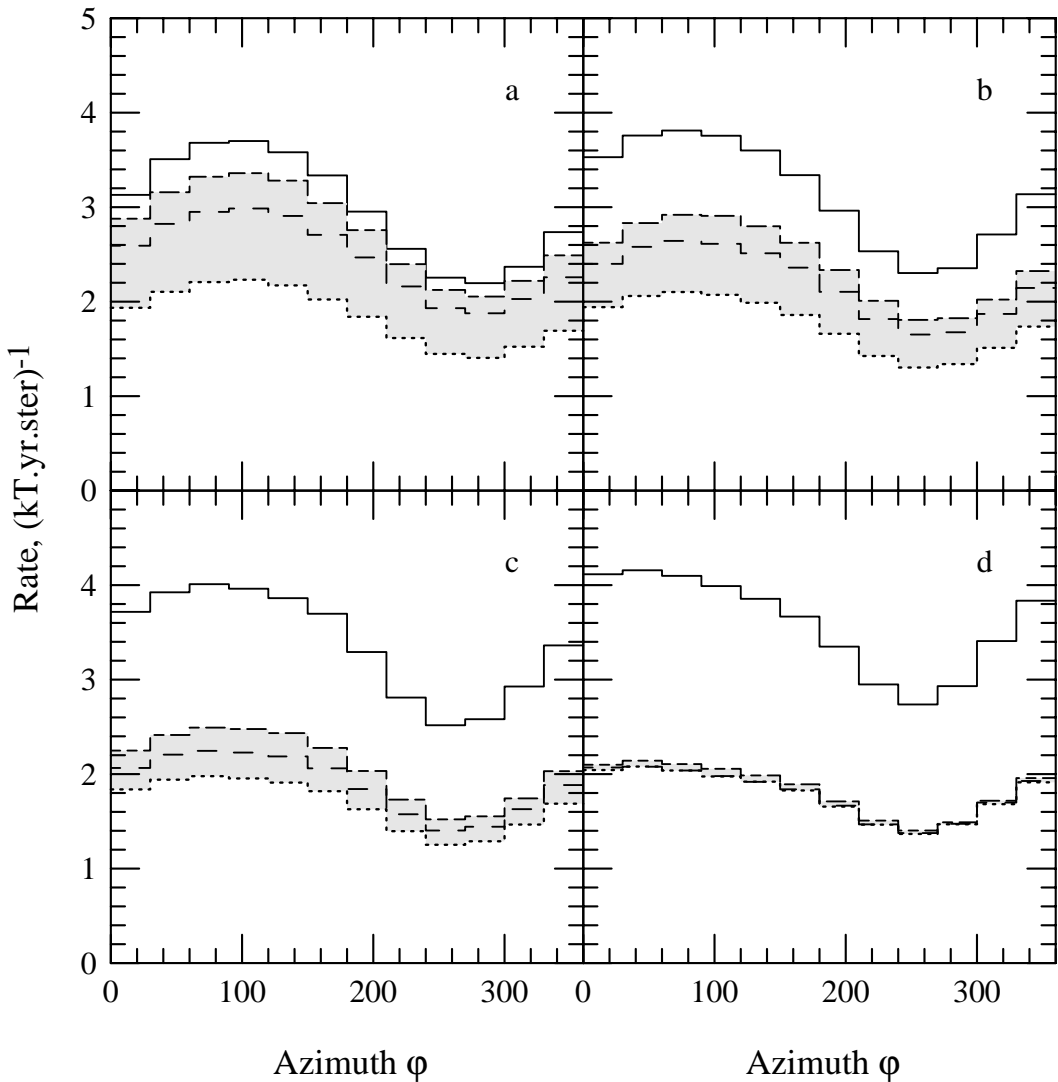


FIG. 6. a) Azimuthal distributions for the sub-GeV muons (see text) at Kamioka for four bins in $\cos \theta_z$: 1 to 0.5 (a); 0.5 to 0. (b); 0. to -0.5 (c); -0.5 to -1. (d) – solid lines. The other histograms show the distributions in the presence of $\nu_\mu \rightarrow \nu_\tau$ oscillations for maximal mixing and $\Delta m^2 = 10^{-2} \text{ eV}^2$ (dots), $10^{-2.5} \text{ eV}^2$ (dashes) and 10^{-3} eV^2 (dash-dash).